Pergamon

Int. J. Heat Mass Transfer. Vol. 38, No. 2, pp. 233–240, 1995

0017-9310/95 $9.50+0.00

0017-9310(94)00155-3

Condensation heat transfer of a non-azeotropic binary mixture on a horizontal tube

W. C. WANG, C. YU and B. X. WANG

Department of Thermal Engineering, Tsinghua University, Beijing 100084, China

(*Received* 12 *January* 1994 *and in final form* 20 *May* 1994)

Abstract—Natural convection condensation heat transfer of a binary HFC152a–HCFC22 mixture on the outside of a horizontal tube was investigated experimentally and analytically. A new model is advanced in which the interface temperature between the liquid and vapor phases is not constant in the flow direction. A non-similarity solution for the flow, temperature and concentration fields on the outside of a smooth horizontal tube is obtained. The calculated results agree well with the experimental results.

1. INTRODUCTION

Condensation heat transfer of nonazeotropic mixtures frequently occurs in the chemical and petroleum industry. It is especially important in the research of CFC alternatives because various non-azeotropic mixtures have been developed.

As shown in Fig. 1, during condensation of a non-azeotropic vapor mixture, the interface temperature between the liquid film and the vapor film will be lower than the dew-point temperature of the vapor flow. Specification of the interface temperature is a key problem. There are many theoretical investigations reported in the literature [1–7], but the interface temperature is normally considered as constant along the flow direction. In 1986, Hijikata [8] first advanced the concept of a pseudo-similar solution when the molecular weight of the low boiling-point component is greater than that of the high boiling-point component. The vapor film thickness developed inversely with that of the condensate film and the interface temperature varied along the flow direction. Later, Zhou [9] numerically obtained a non-similar solution using the finite-difference method. Generally, previous studies had two shortcomings: (1) the constant interface temperature is not applicable; and (2) most of the investigations dealt with vertical plates.

This paper presents analysis and experimental results for condensation heat transfer performance of HFC152a–HCFC22 on a horizontal tube. The condensation heat transfer performance for this mixture compared with that of CFC12 (R12) is of valuable practical significance.

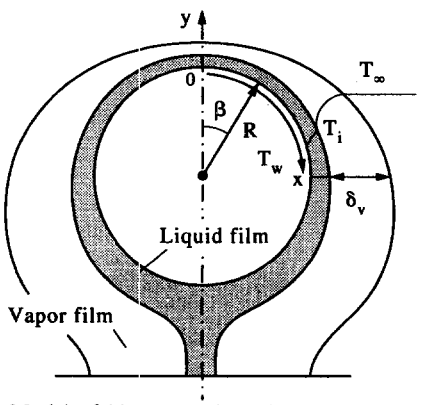

Fig. 1. Model of binary condensation heat transfer on a horizontal tube with curvilinear coordinates.

2. EXPERIMENTAL WORK

All experiments were carried out in a stainless steel vessel, 300 mm diameter, Fig. 2, containing a tube with a 1.2 m long active length. Observation windows

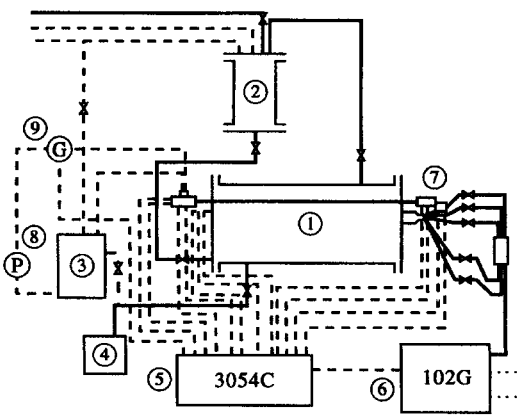

Fig. 2. Experimental apparatus: (1) test vessel; (2) aid condenser; (3) cooling-water vessel; (4) vacuum pump; (5) data acquisition unit; (6) gas-chromatograph; (7) cooling-water mixed chamber; (8) water pump; (9) turbine flowmeter.

NOMENCLATURE

C_p	specific heat [J kg^{-1} °C^{-1}]
D	diffusion coefficient [m^2 s^{-1}]
d	diameter of tube [m]
g	gravitational acceleration [m s^{-2}]
Ga	Galileo number, $Ga = gd^3/v^2$
h	condensation heat transfer coefficient [W m^{-2} °C^{-1}]
H_L	dimensionless phase change number, $H_L = C_p(T_s - T_w)/L_h$
L_h	specific latent heat [J kg^{-1}]
m	mass flux [kg s^{-1}]
M	molecular weight [kg kmol^{-1}]
Nu	Nusselt number
Pr	Prandtl number
Sc	Scimiat number
T	temperature [°C]
u, v	fluid velocity in x- and y-direction, respectively [m s^{-1}]
W	concentration of low boiling-point component [kg kg^{-1}]
x, y	curvilinear coordinates [m].

Greek symbols

δ	thickness of boundary layer [m]
ξ, η	dimensionless variables of coordinate
θ	surplus temperature [°C]
μ	dynamic viscosity [Pa s^{-1}]
v	kinematic viscosity [m^2 s^{-1}]
ψ	flow function [l s^{-1}]
Ω	dimensionless coefficient of buoyancy.

Subscripts

b	bubble-point
d	dew-point
i	interface of liquid and vapor
L	liquid phase
v	vapor phase
∞	infinite.

and a lighting device were set up for visualization of the condensation. A heater for evaporation and a volumetric glass to measure the condensate were installed inside the vessel. The vessel was connected to an external condenser. The non-condensing gases were easily expelled so as to recover the working medium.

The vapor and condensate temperatures were measured by 0.2 mm copper–constantan thermocouples. The average temperature of the tube wall was determined directly by measuring the electrical resistance of the tube itself. The temperature difference between the inlet and outlet cooling water was measured accurately by five copper–constantan thermocouples connected in series. All thermocouples were calibrated in the same constant temperature water bath with an accuracy of ± 0.1°C. The cooling water flow rate was measured by a turbine flowmeter. All signals were transmitted to a HP3054C data acquisition unit (with sensitivity of 0.1 μV). The condensate from the tube flowed through a channel into a volumetric measuring glass. Sample acquisition tubes of 0.8 mm diameter were inserted into the vapor, liquid and condensate regions and connected directly to a gas chromatograph to analyse the composition at each sample point. The volumetric fraction of the non-condensable gas could be controlled to less than 0.01%.

The experiments were carried out for: vapor temperature 35 ± 0.1°C, heat transfer temperature difference between vapor and test tube wall 0.5–10°C, and mass fraction of HCFC22 ranging from 0 to 50%. The heat balance deviation is estimated to be within ± 5% for all experimental data.

3. NUMERICAL ANALYSIS

Numerical analysis has been carried out for the same conditions as in the experimental program. The two-dimensional physical model describing the radius flow is shown in Fig. 1. The basic assumptions are:

(1) the thickness of the vapor film and liquid film are very small compared with the tube radius;
(2) all physical properties, except for the buoyancy, are regarded as constant;
(3) the tube wall temperature is constant around the periphery but not axially;
(4) the vapor stream is saturated and stagnant; and
(5) at the vapor and condensate interface, the multiphase system is always in local equilibrium and, hence, there is no sliding phenomena.

3.1. *Governing equations*

For the nomenclature given in Fig. 3, neglecting viscous dissipation, the governing equations can be written for the condensate and vapor as follows:

Condensate film.

$$\frac{\partial u_L}{\partial x} + \frac{\partial v_L}{\partial y} = 0, \tag{1}$$

$$u_L \frac{\partial u_L}{\partial x} + v_L \frac{\partial u_L}{\partial y} = v_L \frac{\partial^2 u_L}{\partial y^2} + g \sin\left(\frac{2x}{d}\right), \tag{2}$$

$$u_L \frac{\partial T_L}{\partial x} + v_L \frac{\partial T_L}{\partial y} = \left(\frac{\lambda_L}{\rho_L c_{pL}}\right) \frac{\partial^2 T_L}{\partial y^2}. \tag{3}$$

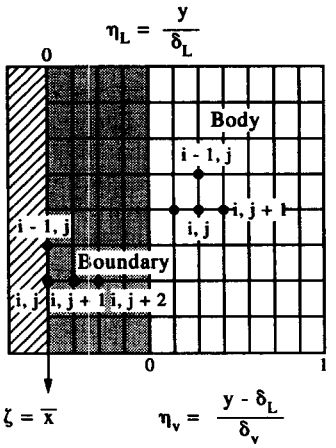

Fig. 3. Finite-difference grid and dimensionless coordinates.

Vapor film.

$$u_v\frac{\partial u_v}{\partial x}+v_v\frac{\partial u_v}{\partial y}=\nu_v\frac{\partial^2 u_v}{\partial y^2}$$
$$+[\Omega_W(W_v-W_{v\infty})+\Omega_T(T_{v\infty}-T_v)$$
$$-\Omega_W\Omega_T(W_v-W_{v\infty})(T_{v\infty}-T_v)]g\sin\left(\frac{2x}{d}\right), \quad (4)$$

$$u_v\frac{\partial T_v}{\partial x}+v_v\frac{\partial T_v}{\partial y}=\frac{\lambda_v}{\rho_v c_{pv}}\frac{\partial^2 T_v}{\partial y^2}, \quad (5)$$

$$u_v\frac{\partial W_v}{\partial x}+v_v\frac{\partial W_v}{\partial y}=D\frac{\partial^2 W_v}{\partial y^2}, \quad (6)$$

$$\Omega_W=\frac{M_1-M_2}{M_1-(M_1-M_2)W_{v\infty}} \quad \Omega_T=\frac{1}{T_{v\infty}}. \quad (7)$$

3.2. *Boundary and initial conditions*

There are three types of boundaries in the present problem: the solid boundary at the wall, the free surface of the vapor film, and the interface boundary between the vapor and the condensate. Hence,

$y = 0$

$$u_L=0, \quad v_L=0, \quad T_L=T_W, \quad (8)$$

$y \to \infty$

$$u_v=u_{v\infty}=0, \quad T_v=T_{v\infty}=T_d, \quad W_v=W_{v\infty}=W_{vd}, \quad (9)$$

$y = \delta_L$

$$u_{Li}=u_{vi}, \quad \left(u_L\frac{\partial u_L}{\partial y}\right)_i=\left(\mu_v\frac{\partial u_v}{\partial y}\right)_i, \quad T_{Li}=T_{vi}=T_i(x), \quad (10)$$

$$\left[\rho_L\left(u_L\frac{d\delta_L}{dx}-v_L\right)\right]_i=\left[\rho_v\left(u_v\frac{d\delta_L}{dx}-v_v\right)\right]_i$$
$$=m_x=m_{1x}+m_{2x}, \quad (11)$$

$$W_{Li}=\frac{m_{1x}}{m_x}, \quad W_{Li}=W_L(T_i,P), \quad W_{vi}=W_v(T_i,P), \quad (12)$$

$$\left(\lambda_L\frac{\partial T_L}{\partial y}\right)_i=L_H m_x+\left(\lambda_v\frac{\partial T_v}{\partial y}\right)_i, \quad (13)$$

$$\left(\rho_v D\frac{\partial W_v}{\partial y}\right)_i=(W_{Li}-W_{vi})m_x. \quad (14)$$

3.3. *Computational method*

The thickness of the condensate film, Π_L, and the thickness of vapor film, δ_v, are the unknown quantities to be determined making it difficult to deal with the grid at the interface. The physical plane was transformed into a computational plane as shown in Fig. 3:

$$\eta_L=\frac{y}{\delta_L}, \quad \eta_v=\frac{y-\delta_L}{\delta_v}, \quad \xi=\frac{x}{d}. \quad (15)$$

Introducing the following dimensionless variables:

$$\bar{u}_L=\frac{u_L d}{\nu_L}, \quad \bar{v}_L=\frac{v_L d}{\nu_L}, \quad \bar{\theta}_L=\frac{T_L-T_W}{T_{v\infty}-T_W},$$
$$\bar{W}_L=\frac{W_L-W_{v\infty}}{W_{vb}-W_{v\infty}}, \quad \bar{u}_v=\frac{u_v d}{\nu_v}, \quad \bar{v}_v=\frac{v_v d}{\nu_v},$$
$$\bar{\theta}_v=\frac{T_{v\infty}-T_v}{T_{v\infty}-T_W}, \quad \bar{W}_v=\frac{W_v-W_{v\infty}}{W_{vb}-W_{v\infty}},$$
$$\bar{\delta}_L=\frac{\delta_L}{d}, \quad \bar{\delta}_v=\frac{\delta_v}{d}, \quad \bar{x}=\frac{x}{d}, \quad \bar{y}=\frac{y}{d}, \quad (16)$$

the dimensionless steam functions, ψ_L and ψ_v, can be defined as:

$$\bar{u}_L=\frac{1}{\bar{\delta}_L}\frac{\partial\bar{\psi}_L}{\partial\eta_L}, \quad \bar{u}_v=\frac{1}{\bar{\delta}_v}\frac{\partial\bar{\psi}_v}{\partial\eta_v}. \quad (17)$$

Equations (1)–(7) can then be defined as:

$$\left(\frac{1}{\bar{\delta}_L}\frac{\partial\bar{\psi}_L}{\partial\eta_L}\right)\frac{\partial\bar{u}_L}{\partial\xi}+\left(-\frac{1}{\bar{\delta}_L}\frac{\partial\bar{\psi}_L}{\partial\xi}\right)\frac{\partial\bar{u}_L}{\partial\eta_L}$$
$$=\left(\frac{1}{\bar{\delta}_L^2}\right)\frac{\partial^2\bar{u}_L}{\partial\eta_L^2}+Ga_L\sin(2\xi), \quad (18)$$

$$\left(\frac{1}{\bar{\delta}_L}\frac{\partial\bar{\psi}_L}{\partial\eta_L}\right)\frac{\partial\bar{\theta}_L}{\partial\xi}+\left(-\frac{1}{\bar{\delta}_L}\frac{\partial\bar{\psi}_L}{\partial\xi}\right)\frac{\partial\bar{\theta}_L}{\partial\eta_L}$$
$$=\left(\frac{1}{Pr_L}\right)\left(\frac{1}{\bar{\delta}_L^2}\right)\frac{\partial^2\bar{\theta}_L}{\partial\eta_L^2}, \quad (19)$$

$$\left(\frac{1}{\bar{\delta}_v}\frac{\partial\bar{\psi}_v}{\partial\eta_v}\right)\frac{\partial\bar{u}_v}{\partial\xi}+\left(-\frac{1}{\bar{\delta}_v}\frac{\partial\bar{\psi}_v}{\partial\xi}\right)\frac{\partial\bar{u}_v}{\partial\eta_v}=\left(\frac{1}{\bar{\delta}_v^2}\right)\frac{\partial^2\bar{u}_v}{\partial\eta_v^2}$$
$$+[Ga_v\sin(2\xi)][\Omega_w\bar{W}_v(W_{vb}-W_{v\infty})+\Omega_T\bar{\theta}_v(T_{v\infty}-T_w)$$
$$-\Omega_w\Omega_T\bar{W}_v\bar{\theta}_v(W_{vb}-W_{v\infty})(T_{v\infty}-T_w)], \quad (20)$$

$$\left(\frac{1}{\bar{\delta}_v}\frac{\partial\bar{\psi}_v}{\partial\eta_v}\right)\frac{\partial\bar{\theta}_v}{\partial\xi}+\left(-\frac{1}{\bar{\delta}_v}\frac{\partial\bar{\psi}_v}{\partial\xi}\right)\frac{\partial\bar{\theta}_v}{\partial\eta_v}=\left(\frac{1}{Pr_v}\right)\left(\frac{1}{\bar{\delta}_v^2}\right)\frac{\partial^2\bar{\theta}_v}{\partial\eta_v^2}. \tag{21}$$

$$\left(\frac{1}{\bar{\delta}_v}\frac{\partial\bar{\psi}_v}{\partial\eta_v}\right)\frac{\partial\bar{W}_v}{\partial\xi}+\left(-\frac{1}{\bar{\delta}_v}\frac{\partial\bar{\psi}_v}{\partial\xi}\right)\frac{\partial\bar{W}_v}{\partial\eta_v}=\left(\frac{1}{Sc_v}\right)\left(\frac{1}{\bar{\delta}_v^2}\right)\frac{\partial^2\bar{W}_v}{\partial\eta_v^2}, \tag{22}$$

The corresponding boundary conditions are:

$\eta_L=0$

$$\bar{u}_L=0,\quad \bar{\psi}_L=0,\quad \bar{\theta}_L=0; \tag{23}$$

$\delta_v\to\infty,\quad \eta_v=1$

$$\bar{u}_v=0,\quad \bar{\theta}_v=0,\quad \bar{W}_v=0; \tag{24}$$

$\eta_L=1,\quad \eta_v=0$

$$\nu_L\bar{u}_{Li}=\nu_v\bar{u}_{vi},\quad \bar{\theta}_{Li}+\bar{\theta}_{vi}=1, \tag{25}$$

$$\bar{W}_{Li}=\bar{W}_L(\bar{\theta}_{Li},P),\quad \bar{W}_{vi}=\bar{W}_v(\bar{\theta}_{vi},P), \tag{26}$$

$$\left(\frac{\partial\bar{u}_L}{\partial\eta_L}\right)_i=\left(\frac{\mu_v\nu_v}{\mu_L\nu_L}\right)\left(\frac{\delta_L}{\delta_v}\right)\left(\frac{\partial\bar{u}_v}{\partial\eta_v}\right), \tag{27}$$

$$\left(\frac{\partial\bar{\psi}_L}{\partial\xi}\right)_i=\frac{\mu_v}{\mu_L}\left(\frac{\partial\bar{\psi}_v}{\partial\xi}\right)_i=\bar{m}_{xL}, \tag{28}$$

$$\frac{1}{\bar{\delta}_L}\left(\frac{\partial\bar{\theta}_L}{\partial\eta_L}\right)_i=\frac{Pr_L\bar{m}_{xL}}{H_L}-\left(\frac{\lambda_v}{\lambda_L}\right)\left(\frac{1}{\bar{\delta}_v}\right)\left(\frac{\partial\bar{\theta}_v}{\partial\eta_v}\right), \tag{29}$$

$$\frac{1}{\bar{\delta}_v}\left(\frac{\partial\bar{W}_v}{\partial\eta_v}\right)_i=\bar{m}_{xv}Sc_v(\bar{W}_{Li}-\bar{W}_{vi}). \tag{30}$$

For $\beta=0$ (defined in Fig. 1):

$$\bar{u}_L=0,\quad \bar{u}_V=0,\quad \frac{\partial\bar{\theta}_L}{\partial\xi}=0,\quad \frac{\partial\bar{\theta}_v}{\partial\xi}=0,\quad \frac{\partial\bar{W}_v}{\partial\xi}=0. \tag{31}$$

Equations (18)–(22) can be linearized into the following common form:

$$A\frac{\partial\phi}{\partial\xi}+B\frac{\partial\phi}{\partial\eta}=C\frac{\partial^2\phi}{\partial\eta^2}+D. \tag{32}$$

Equation (32) can be discretized using the finite difference grid shown in Fig. 3. The step lengths for ξ, η_L and η_v were all 1/50. For each partial difference equation, a group of linear equations was obtained with a tridigonal coefficient matrix. The computational scheme is shown in Fig. 4.

4. RESULT AND DISCUSSION

Figure 5 compares the velocity distribution profiles for different tube–vapor temperature differences for a HCFC22 concentration of 50% in the vapor. For small temperature differences, Fig. 5(a), the maximum vapor film velocity is greater than that of the condensate film velocity at the same section. The shear stress in the vapor film at the liquid–vapor interface is counter to the vapor flow direction, acting to resist the vapor film flow at the interface. Therefore, the motive force for the vapor film flow is the buoyancy caused by the concentration difference and the temperature difference. On the contrary, for larger temperature differences in Fig. 5(c), the shear stress in the vapor film at the interface is in the flow direction and is the main motive force of the vapor film flow. The buoyancy has little effect on the vapor flow.

For the temperature distribution, Fig. 6, the interface temperature decreases along the periphery, with an especially sharp decrease near the bottom of the tube Fig. 6(a) and (b). When the concentration of HCFC22 is small and the temperature difference is very large, the interface temperature is nearly uniform along the periphery, Fig. 6(c). Thus, there are two types of low boiling-point component accumulation effects at the interface between condensate and vapor, in the radial and circumferential directions. When the temperature difference is small, these two types of accumulation effects are of the same order. When the temperature difference is great, the circumferent accumulation effect is negligible; there is only a radial concentration gradient at the interface. Figure 7 shows the average interface temperature distribution for different temperature differences between the tube and the vapor. The interface temperature sharply decreases with increasing temperature difference and quickly approaches the bubble-point temperature for the specified total pressure.

Figures 8–10 compare the distribution of the average condensation heat transfer coefficient, the average total heat transfer resistance and the vapor film heat transfer resistance, and the condensate film heat transfer resistance. For smaller tube–vapor temperature differences or larger HCFC22 concentrations, the vapor film heat transfer resistance caused by the mass transfer increases and the heat transfer continues to decrease. For the same concentration, there is a maximum average heat transfer coefficient. The temperature difference (T_s-T_w) corresponding to the maximum heat transfer coefficient gradually increases with increasing HCFC22 concentration. For the same temperature difference, there is a minimum average condensation heat transfer coefficient. Figure 11 compares numerical results and experimental data which agreed well for small HCFC22 concentrations and deviated 20% for large concentrations.

5. CONCLUSIONS

(1) A new heat transfer model for condensation of a binary non-azeotropic mixture on horizontal tubes is advanced in which the condensate–vapor interface temperature is not constant along the flow direction regardless of whether the molecular weight of the low boiling-point component is greater or smaller than that of the high boiling-point component. The non-similarity solutions for the flow, temperature and con-

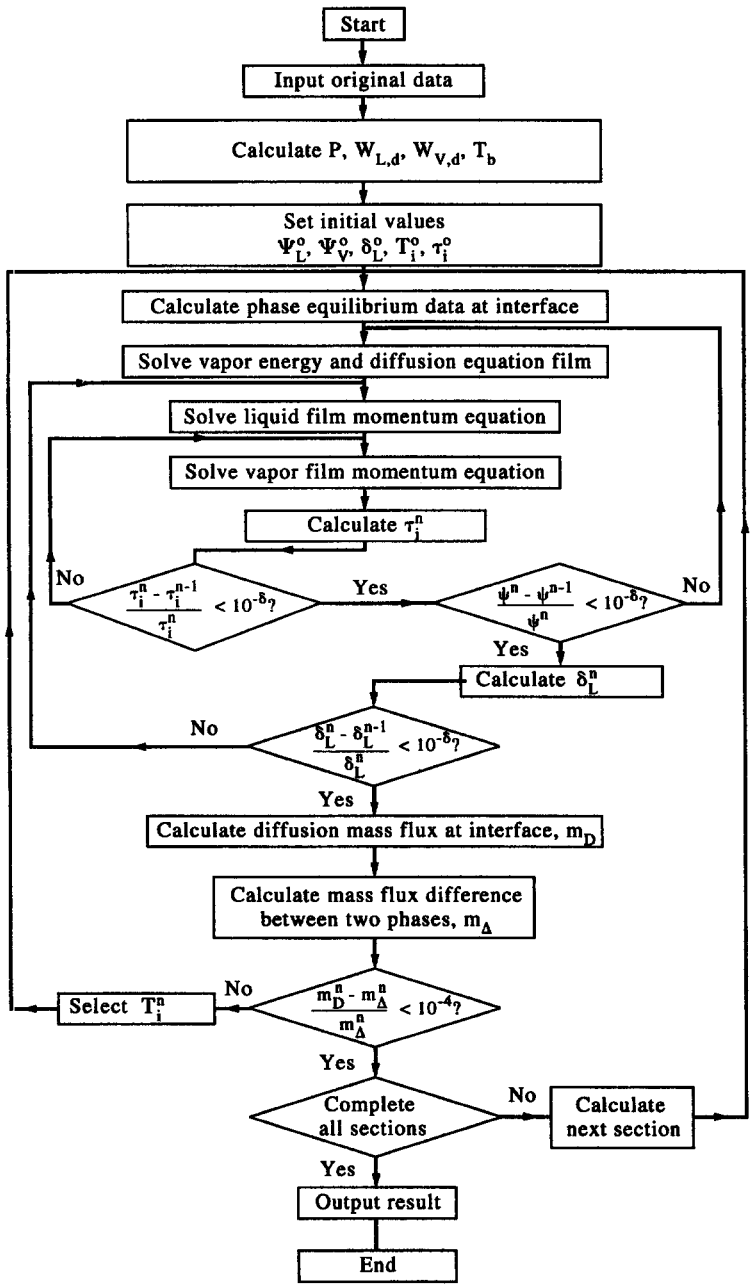

Fig. 4. Iteration scheme.

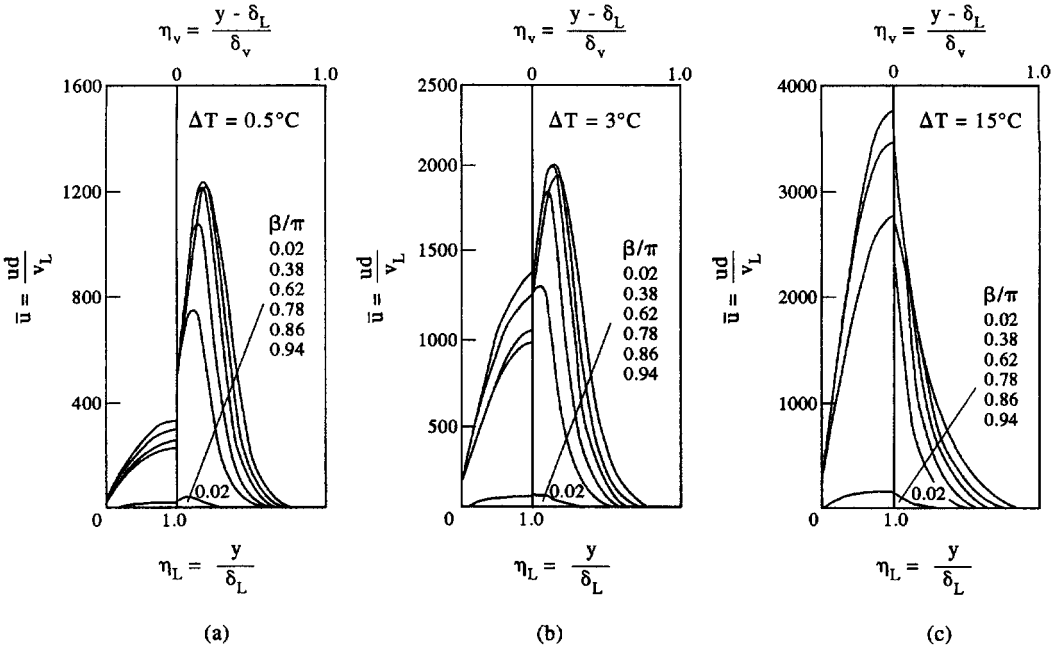

Fig. 5. Velocity distribution profiles for different temperature differences for HCFC22 concentration of 50%.

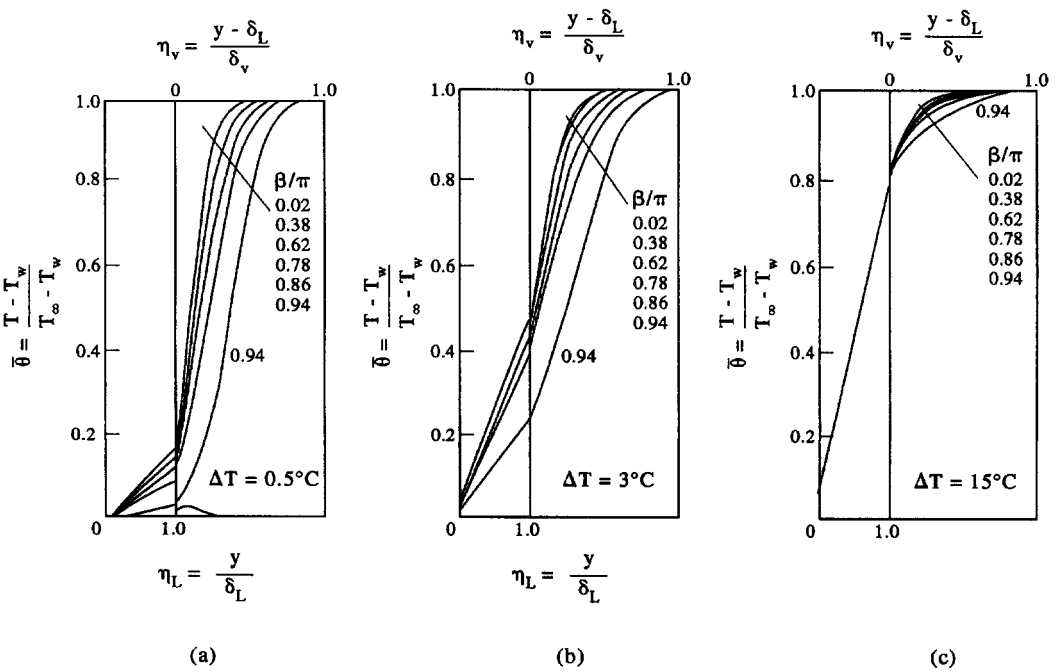

Fig. 6. Temperature distribution profiles for different temperature differences for HCFC22 concentration of 50%.

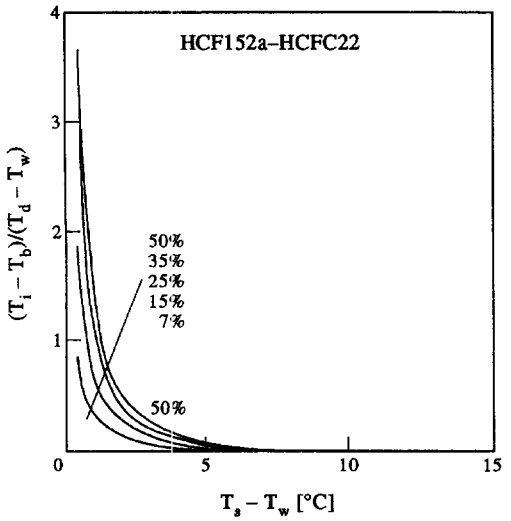

Fig. 7. Average interface temperature distributions.

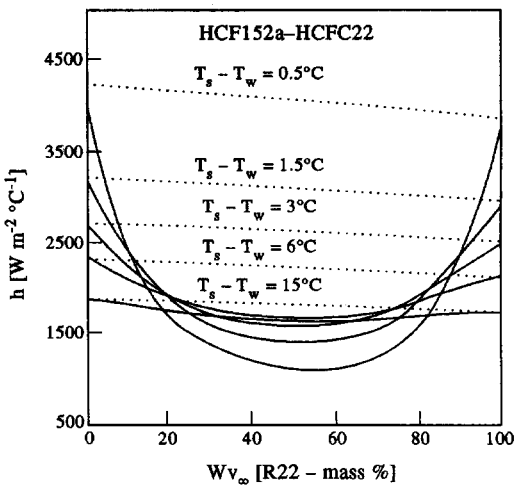

Fig. 10. Average heat transfer coefficient distribution for various concentrations.

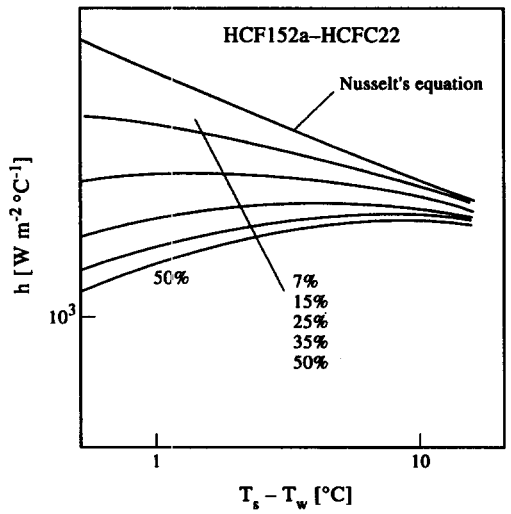

Fig. 8. Average heat transfer coefficient distributions.

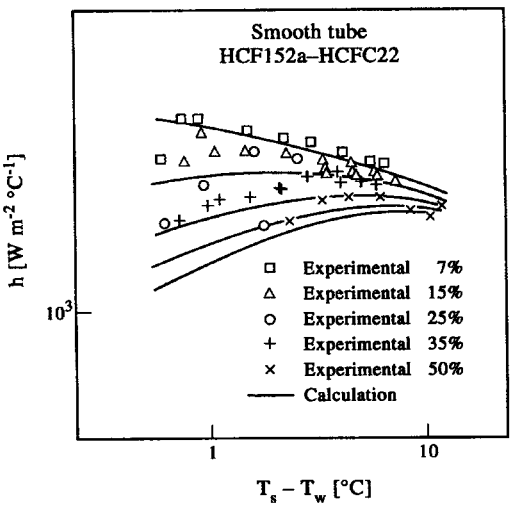

Fig. 11. Comparison of experimentally measured and calculated condensation heat transfer coefficients.

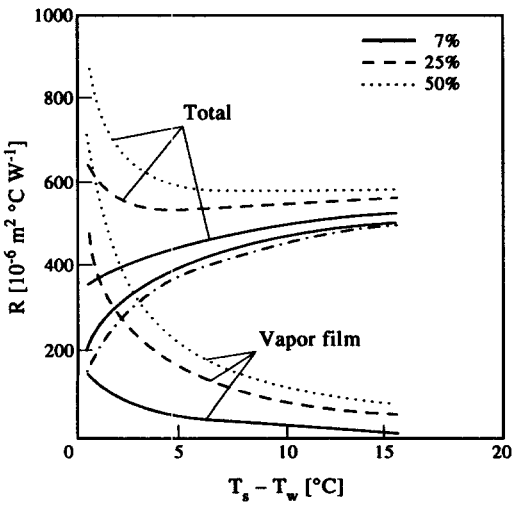

Fig. 9. Comparison of total heat transfer resistance and vapor film heat resistance.

centration fields have been obtained using the finite difference method.

(2) Mixtures of HFC152a–HCFC22 have been analysed numerically. The predicted condensation heat transfer performance agreed well with the experimental results.

(3) Analysis showed that the condensate–vapor interface temperature decreased along the flow direction and that the average heat transfer coefficient reached a maximum as the tube–vapor temperature difference increased at constant HCFC22 concentration.

(4) Both the analytical and experimental results show that the heat transfer deteriorated when HCFC22 was added to HFC152a. However, the condensation heat transfer performance of the mixture is not lower than that of pure CFC12 for some ranges of concentration and tube–vapor temperature difference.

REFERENCES

1. E. M. Sparrow and E. R. G. Eckert, Effects of superheated vapor and noncondensable gases on laminar film condensation, *A.I.Ch.E. Jl* **7**(3), 473–477 (1961).
2. E. M. Sparrow and S. H. Lin, Condensation heat transfer in the presence of a noncondensable gas, *ASME J. Heat Transfer* **8**(3), 430–436 (1964).
3. W. J. Minkowycz and E. M. Sparrow, Condensation heat transfer in the presence of noncondensables, interfacial resistance, superheating, variable properties and diffusion, *Int. J. Heat Mass Transfer* **9**, 1125–1144 (1966).
4. E. M. Sparrow and E. Marshall, Binary, gravity-flow film condensation, *ASME J. Heat Transfer* **91**(2), 205–211 (1969).
5. V. F. Chaikovskii, G. F. Sminov and R. A. Domanskii, Study of condensation of a two-component mixtures of Freon 12 and Freon 22, *Heat Transfer—Soviet Res.* **4**(6), 80–83 (1972).
6. A Tamir, Condensation of binary mixtures of miscible vapors, *Int. J. Heat Mass Transfer* **16**, 683–685 (1973).
7. T. Fujii, H. Uehara, K. Mihara and H. Takashima, Body force convection condensation in the presence of noncondensables (in Japanese), *Reports of Research Institute of Industrial Science, Kyushu University* **67**, 23–41 (1978).
8. K. Hijikata, Y. Mori, N. Himeno, M. Inagawa and K. Takahasi, Free convective filmwise condensation of a binary of vapors. In *Proc. Eighth International Heat Transfer Conference*, San Francisco, **4**, 1621–1626 (1986).
9. Y. Q. Zhou and K. Hijikata, Non-similar solution of natural convection condensation heat transfer of binary mixture vapors, *Trans. JSME*, **56(B)**, 136–141 (1990).
10. T. Fujii, *Theory of Laminar Film Condensation*. Springer-Verlag, New York (1991).
11. J. M. Prousnize, R. N. Lichenthaler and E. G. Azevedo, *Molecular Thermodynamics of Fluid-Phase Equilibria* (2nd Edn). Prentice-Hall, Englewood Cliffs, NJ (1986).
12. W. C. Wang, L. N. Zhang, Chao Yu and C. J. Gan, Experimental study of the condensation heat transfer of HFC152a/HCFC22 on the horizontal tube. In *Proceedings of International Conference on CFC and HALAN Alternatives*, Beijing, China, pp. 251–255 (1993).